Physica A 387 (2008) 5979–5990

Contents lists available at ScienceDirect

Physica A

journal homepage: www.elsevier.com/locate/physa

Pressure-driven transient flows of Newtonian fluids through microtubes with slip boundary

Yong Hong Wu [a,*], B. Wiwatanapataphee [b,*], Maobin Hu [c]

[a] Department of Mathematics and Statistics, Curtin University of Technology, Perth, WA 6845, Australia
[b] Department of Mathematics, Faculty of Science, Mahidol University, Bangkok 10400, Thailand
[c] School of Engineering Science, University of Science and Technology of China, China

ARTICLE INFO

Article history:
Received 12 March 2008
Received in revised form 16 May 2008
Available online 4 July 2008

Keywords:
Fluid flow
Microtube
Slip boundary condition
Navier–Stokes equations
Flow rate

ABSTRACT

Recent advances in microscale experiments and molecular simulations confirm that slip of fluid on solid surface occurs at small scale, and thus the traditional no-slip boundary condition in fluid mechanics cannot be applied to flow in micrometer and nanometer scale tubes and channels. On the other hand, there is an urgent need to understand fluid flow in micrometer scale due to the emergence of biochemical lab-on-the-chip system and micro-electromechanical system fabrication technologies. In this paper, we study the pressure driven transient flow of an incompressible Newtonian fluid in microtubes with a Navier slip boundary condition. An exact solution is derived and is shown to include some existing known results as special cases. Through analysis of the derived solution, it is found that the influences of boundary slip on the flow behaviour are qualitatively different for different types of pressure fields driving the flow. For pressure fields with a constant pressure gradient, the boundary slip does not alter the interior material deformation and stress field; while, for pressure fields with a wave form pressure gradient, the boundary slip causes the change of interior material deformation and consequently the velocity profile and stress field. We also derive asymptotic expressions for the exact solution through which a parameter $\bar{\beta}$ is identified to dominate the behaviour of the flow driven by the wave form pressure gradient, and an explicit formulae for the critical slip parameter leading to the maximum transient flow rate is established.

1. Introduction

Within the past decade, one of the important scientific research focuses worldwide has been on the study of the behaviour of materials at micro and nanoscales. Advances from the research community in this area led to the development of many biological and engineering devices and systems in microscale and nanoscale [12]. Most of these devices and systems involve fluid flow through microchannels, referred to as microflows [1,9,8,10]. Typical examples include fuel cell devices, drug delivery systems [23], biological sensing and energy conversion devices [16]. As the behaviour of fluid flow in these systems determines the functional characteristics of the systems, the study of microflows is attracting more and more attention from the science and engineering communities in order to derive a better understanding of the mechanism of microflows and develop better models [7].

For the flow of incompressible Newtonian fluids, the governing field equations are the incompressible continuity equation and the Navier–Stokes equations. In addition, a boundary condition has to be imposed on the field equations.

* Corresponding author. Tel.: +61 8 92663142.
E-mail addresses: yhwu@maths.curtin.edu.au (Y.H. Wu), scbww@mahidol.ac.th (B. Wiwatanapataphee).

0378-4371/$ – see front matter © 2008 Elsevier B.V. All rights reserved.
doi:10.1016/j.physa.2008.06.043

Traditionally the so-called no-slip boundary condition is used, namely the fluid velocity relative to the solid is zero on the fluid–solid interface [22]. However, the no-slip condition is a hypothesis rather than a condition deduced from any principle, and thus its validity has been continuously debated in the scientific literature. Although many experimental results were shown to support the no-slip condition including those by Coulomb and Couette, evidences of slip of a fluid on a solid surface were also reported by many others [18]. Chauveteau [5], Tuinier and Taniguchi [26], and Vargas and Manero [27] studied the flow of polymer solutions in porous media and showed that the apparent viscosity of the fluids near the wall is lower than that in the bulk and consequently the fluids can exhibit the phenomenon of apparent slip on the wall. More recently, experiments in micrometer scale and molecular dynamic simulations were carried out to investigate the nature of fluid interaction with the solid surface [3]. It has now been established that the interaction of fluid with the solid surface of microchannels is very different from that in large systems, due to the large ratio of surface area with volume for the microsystems. The flow of fluids in microsystems is granular and slip can occur [2,24,31,36]. Hence, the no-slip condition is not acceptable for fluid flows in microchannels although it is applicable to fluid flows in large systems.

To describe the slip characteristics of fluid on the solid surface, Navier introduced a more general boundary condition, namely the fluid velocity component tangential to the solid surface, relative to the solid surface, is proportional to the shear stress on the fluid–solid interface. The proportionality is called the slip length which describes the "slipperiness" of the surface [33,13]. Although Navier's slip condition was proposed about two hundreds year ago, it attracts significant attention of the science and engineering communities only very recently for the study of flows in microscale. Recent advances in the manufacture of microdevices enable experimental investigation of fluid flow in microscale, and many experimental results have provided evidences to support the Navier slip condition [11,33,18]. Some attempts have also been made to use nanotechnologies for the surface treatment of microchannels so as to achieve large slip for maximizing the transport efficiency of fluids through microchannels. Over the last few years, various investigations have also been made to study various flow problems of Newtonian and non-Newtonian fluids with Navier slip boundary condition [6,14,21,20,17,34,35]. Some attempts have also been made to derive alternative formulae for the determination of the slip length [25].

Although exact and numerical solutions to various flow problems of Newtonian fluids under the no-slip assumption have been obtained and are available in literature [22,30,28,29], very few exact solutions for the slip case are available in literature. Recently, some steady state slip solutions for the flows through a pipe, a channel and an annulus have been obtained [32, 15]. In this paper, we will derive a new exact solution for the transient flow of Newtonian fluids in microtubes with a slip boundary condition, and then discuss the influence of the slip length on the velocity field as well as the stress field in the fluid. The rest of the paper is organized as follows. In the following section, we first define the problem and then present its mathematical formulation. In Section 3, we solve the underlying boundary value problem to derive the exact solution for the velocity field and show that the solution includes some existing known solutions as special cases. In Section 4, we derive exact solutions for the flow rate, the rate of deformation tensor and the stress field in the fluid using the exact solution of velocity field derived in Section 3. In Section 5, an analysis is carried out to study the influence of the slip parameter on the flow behaviour. Finally a conclusion is given in Section 6.

2. Problem description and mathematical formulation

Consider the transient flow of an incompressible Newtonian fluid through a circular microtube with the z-axis being in the axial direction. The field equations governing the flow include the continuity equation and the Navier–Stokes equations as given below

$$\nabla \cdot \mathbf{v} = 0, \tag{1}$$

$$\frac{\partial \mathbf{v}}{\partial t} + (\mathbf{v} \cdot \nabla)\mathbf{v} = \mathbf{f} - \frac{1}{\rho}\nabla p + \frac{\mu}{\rho}\nabla^2 \mathbf{v}, \tag{2}$$

where p and $\mathbf{v}$ are respectively the fluid pressure and velocity vector, ∇ and ∇^2 represent the gradient operator and the Laplace operator respectively, the dot $\cdot$ between two vector quantities represents the scalar product operation, $\mathbf{f}$ is the body force acting on the fluid, ρ and μ are respectively the fluid density and viscosity. The stress field in the fluid is related to the velocity field by the following constitutive equation

$$\sigma = -pI + 2\mu\mathbf{d}, \tag{3}$$

while the rate of deformation tensor is related to the velocity vector by

$$\mathbf{d} = \frac{1}{2}(\nabla\mathbf{v} + (\nabla\mathbf{v})^{\mathrm{T}}), \tag{4}$$

where $\sigma = (\sigma_{ij})$ and $\mathbf{d} = (d_{ij})$ denote respectively the second-order stress tensor and the rate of deformation tensor, and I is an identity matrix.

In cylindrical polar coordinates (r, θ, z), $\mathbf{v} = \mathbf{e}_r v_r + \mathbf{e}_\theta v_\theta + \mathbf{e}_z u$ and the gradient operator is

$$\nabla = \mathbf{e}_r \frac{\partial}{\partial r} + \mathbf{e}_\theta \frac{\partial}{r\partial r} + \mathbf{e}_z \frac{\partial}{\partial z}, \tag{5}$$

where $\mathbf{e}_r$, $\mathbf{e}_\theta$ and $\mathbf{e}_z$ are respectively the radial unit vector, the transverse unit vector and the axial unit vector. Thus, the continuity equation and the Navier–Stokes equation along the axial (z) direction can be written as

$$\frac{1}{r}\frac{\partial}{\partial r}(rv_r) + \frac{1}{r}\frac{\partial v_\theta}{\partial \theta} + \frac{\partial u}{\partial z} = 0, \tag{6}$$

$$\rho\left(\frac{\partial u}{\partial t} + u\frac{\partial u}{\partial z} + v_r\frac{\partial u}{\partial r} + \frac{v_\theta}{r}\frac{\partial u}{\partial \theta}\right) = \rho g_z - \frac{\partial p}{\partial z} + \mu\left(\frac{\partial^2 u}{\partial z^2} + \frac{1}{r}\frac{\partial}{\partial r}\left(r\frac{\partial u}{\partial r}\right) + \frac{1}{r^2}\frac{\partial^2 u}{\partial \theta^2}\right). \tag{7}$$

As the flow is axially symmetric, there is no swirling flow and the velocity components in the radial and transverse directions vanish, namely

$$v_r = 0, \qquad v_\theta = 0. \tag{8}$$

Substituting the above into the continuity Eq. (6) yields

$$\frac{\partial u}{\partial z} = 0, \tag{9}$$

which gives rise to $u = u(r, \theta)$. Further, $g_z = 0$, as the flow is horizontal, and hence Eq. (7) becomes

$$\frac{\mu}{\rho}\left(\frac{\partial^2 u}{\partial r^2} + \frac{1}{r}\frac{\partial u}{\partial r}\right) - \frac{\partial u}{\partial t} = \frac{1}{\rho}\frac{\partial p}{\partial z}. \tag{10}$$

In this work, we consider the fluid flow driven by the pressure field with a pressure gradient $\bar{q}(t)$ that can be expressed by the Fourier series, namely

$$\frac{\partial p}{\partial z} = \bar{q}(t) = a_0 + \sum_{n=1}^{\infty}[a_n \cos(n\omega t) + b_n \sin(n\omega t)]. \tag{11}$$

Remark 2.1. As a wide range of functions can be expressed in terms of Fourier series, the assumption of the form of pressure gradient (11) will not lose generality. However, it should be addressed here that our work is limited to the cases where the pressure gradient varies with time only.

Remark 2.2. Flow of fluids driven by non-constant pressure gradient occurs in many natural and industrial processes. A typical example is the pulsatile blood flow through arteries in which the pressure gradient driving the flow of blood is in pulsatile form [29]. It should also be addressed here that various methods can be used to generate pulsatile flows, such as those by using reciprocating pistons, servo valves or air pulsation [4,19].

For convenience in deriving analytical solutions of the field equations, we use complex number to express (11) by exponential functions, namely

$$\frac{\partial p}{\partial z} = \mathrm{Re}\left(\sum_{n=0}^{\infty} c_n e^{in\omega t}\right), \tag{12}$$

where

$$c_n = a_n - b_n i, \qquad e^{in\omega t} = \cos(n\omega t) + i\sin(n\omega t).$$

To completely define the problem, the field equations must be supplemented by the boundary condition. In this work, we use the Navier slip boundary condition. That is, on the solid–fluid interface $r = R$, the axial fluid velocity, relative to the solid surface, is proportional to the shear stress on the interface. Assume that the rigid microtube moves with an axial velocity $\bar{v}_t(t)$, then the Navier slip condition can be written as

$$u(R, t) - \bar{v}_t(t) = -l\frac{\sigma_{rz}(R, t)}{\mu}, \tag{13}$$

where μ is the fluid viscosity and l is the so-called slip length, the negative sign on the right-hand side of the above equation is to reflect that the shear stress on the interface is always in the opposite direction of the axial fluid velocity as any tangential movement of a fluid particle relative to the solid surface will always be restricted by a resistance force acting on the opposite direction of the relative movement, $\sigma_{rz}(R, t)$ is the shear stress on the interface between the fluid and the wall of the microtube. It should be addressed here that for $l = 0$, condition (13) reduces to the no-slip boundary condition; while, for $l \to \infty$, Eq. (13) gives a surface traction condition for a perfectly smooth surface, i.e, $\sigma_{rz}(R, t) = 0$. For the problem under consideration here, we assume that the microtube is fixed spatially, i.e. $\bar{v}_t(t) = 0$. Thus by noting that $\sigma_{rz}(R, t) = \mu\frac{\partial u}{\partial r}$, we have from Eq. (13) that

$$u(R, t) = -l\frac{\partial u}{\partial r}(R, t). \tag{14}$$

3. Exact solution for the transient velocity field

As Eq. (10) is a linear equation, we can use the superposition principle for the solution of the equation. That is, if u_n is the solution of (10) for $\partial p/\partial z = c_n e^{in\omega t}$, then the complete solution of (10) for $\frac{\partial p}{\partial z} = \mathrm{Re}\left(\sum_{n=0}^{\infty} c_n e^{in\omega t}\right)$ is $u = \sum_{n=0}^{\infty} \mathrm{Re}(u_n)$.

To determine u_n, we solve

$$\frac{\mu}{\rho}\left(\frac{\partial^2 u_n}{\partial r^2} + \frac{1}{r}\frac{\partial u_n}{\partial r}\right) - \frac{\partial u_n}{\partial t} = \frac{c_n}{\rho} e^{in\omega t}, \tag{15}$$

which admits solutions of the form

$$u_n = f_n(r) e^{in\omega t}. \tag{16}$$

Substituting the above equation into (15) yields

$$\frac{\mu}{\rho}\left(\frac{\partial^2 f_n}{\partial r^2} + \frac{1}{r}\frac{\partial f_n}{\partial r}\right) e^{in\omega t} - in\omega f_n e^{in\omega t} = \frac{c_n}{\rho} e^{in\omega t}. \tag{17}$$

For $n = 0$, Eq. (17) becomes

$$r^2\frac{\partial^2 f_0}{\partial r^2} + r\frac{\partial f_0}{\partial r} = \frac{c_0}{\mu} r^2, \tag{18}$$

which has the general solution

$$f_0(r) = (A_1 + A_2 \ln r) + \frac{c_0}{4\mu} r^2.$$

As the solution $f(r)$ must be bounded ar $r = 0$, we require $A_2 = 0$ and hence, we obtain

$$u_0 = f_0(r) = A_1 + \frac{c_0}{4\mu} r^2. \tag{19}$$

For $n \geq 1$, Eq. (17) gives

$$\frac{1}{\beta_n^2}\frac{\partial^2 f_n}{\partial r^2} + \frac{1}{\beta_n^2 r}\frac{\partial f_n}{\partial r} + f_n = \frac{c_n}{\beta_n^2 \mu}, \tag{20}$$

where $\beta_n^2 = n\beta^2$ in which $\beta^2 = -\frac{\rho\omega}{\mu} i$. Let $\bar{r} = \beta_n r$, then Eq. (20) becomes

$$\bar{r}^2\frac{\partial^2 f_n}{\partial \bar{r}^2} + \bar{r}\frac{\partial f_n}{\partial \bar{r}} + \bar{r}^2 f_n = \frac{c_n}{\beta_n^2 \mu}\bar{r}^2. \tag{21}$$

The associated homogeneous equation of the above equation is the zero-order Bessel equation and thus has the following solution

$$f_{nc} = d_n J_0(\bar{r}) + e_n Y_0(\bar{r}) = d_n J_0(\beta_n r) + e_n Y_0(\beta_n r), \tag{22}$$

where d_n and e_n are integration constants, J_0 and Y_0 denote the zero-order Bessel functions of the first kind and the second kind respectively. As f_{nc} must be bounded in the computation domain but $Y_0(\beta_n r)$ has singularity at $r = 0$, we require that $e_n = 0$.

To find the particular solution corresponding to the driving force, we let $f_{nc} = C$, and then by substituting it into (20), we have $C = \frac{c_n i}{\rho n\omega}$. Hence, the general solution of (20) is

$$f_n = f_{nc} + f_{np} = d_n J_0(\beta_n r) + \frac{c_n i}{\rho n\omega}. \tag{23}$$

From (16), (19) and (23) and the superposition principle, we have

$$u = \mathrm{Re}\left(A_1 + \frac{c_0}{4\mu} r^2\right) + \sum_{n=1}^{\infty} \mathrm{Re}\left[\left(d_n J_0(\beta_n r) + \frac{c_n i}{\rho n\omega}\right) e^{in\omega t}\right].$$

As $c_0 = a_0 - ib_0$, we have from the above equation that

$$u = A_1 + \frac{a_0}{4\mu} r^2 + \sum_{n=1}^{\infty} \mathrm{Re}\left[\left(d_n J_0(\beta_n r) + \frac{c_n i}{\rho n\omega}\right) e^{in\omega t}\right]. \tag{24}$$

Consequently we obtain

$$\frac{\partial u}{\partial r} = \frac{a_0}{2\mu} r + \sum_{n=1}^{\infty} \mathrm{Re}\left(-d_n \beta_n J_1(\beta_n r) \mathrm{e}^{\mathrm{i}n\omega t}\right), \tag{25}$$

where, in the above formulation, we have used the identity

$$\frac{\mathrm{d}J_0(x)}{\mathrm{d}x} = -J_1(x).$$

Substituting (24) and (16) into boundary condition (14) yields

$$\left(A_1 + \frac{a_0}{4\mu} R^2 + l\frac{a_0}{2\mu} R\right) + \sum_{n=1}^{\infty} \mathrm{Re}\left[\left(d_n J_0(\beta_n R) + \frac{c_n \mathrm{i}}{\rho n\omega} - l\beta_n d_n J_1(\beta_n r)\right) \mathrm{e}^{\mathrm{i}n\omega t}\right] = 0. \tag{26}$$

For the above equation to hold for any instant of time t, we require that the constant term and the coefficients of $\mathrm{e}^{\mathrm{i}n\omega t}$ all vanish, namely

$$A_1 + \frac{a_0}{4\mu} R^2 + l\frac{a_0}{2\mu} R = 0$$

and

$$d_n[J_0(\beta_n R) - l\beta_n J_1(\beta_n R)] + \frac{c_n \mathrm{i}}{\rho n\omega} = 0,$$

which give

$$A_1 = -\frac{a_0 R^2}{4\mu}\left(1 + \frac{2l}{R}\right), \tag{27}$$

$$d_n = \frac{-c_n \mathrm{i}}{\rho n\omega[J_0(\beta_n R) - l\beta_n J_1(\beta_n R)]}. \tag{28}$$

Hence, by substituting (27) and (28) into (24), we obtain

$$u = -\frac{a_0 R^2}{4\mu}\left[1 - \left(\frac{r}{R}\right)^2 + \frac{2l}{R}\right] - \sum_{n=1}^{\infty} \mathrm{Re}\left[\frac{c_n \mathrm{i}}{\rho n\omega}\left(\frac{J_0(\beta_n r)}{J_0(\beta_n R) - l\beta_n J_1(\beta_n R)} - 1\right) \mathrm{e}^{\mathrm{i}n\omega t}\right]. \tag{29}$$

Remark 3.1. If $l = 0$, solution (29) becomes

$$u = -\frac{a_0 R^2}{4\mu}\left[1 - \left(\frac{r}{R}\right)^2\right] - \sum_{n=1}^{\infty} \mathrm{Re}\left[\frac{c_n \mathrm{i}}{\rho n\omega}\left(\frac{J_0(\beta_n r)}{J_0(\beta_n R)} - 1\right) \mathrm{e}^{\mathrm{i}n\omega t}\right], \tag{30}$$

which is the solution for the no-slip case.

Remark 3.2. If $l \gg R$ and is sufficiently large, solution (29) can be approximated by

$$u \approx -\frac{a_0 l R}{2\mu} + \sum_{n=1}^{\infty} \mathrm{Re}\left(\frac{c_n \mathrm{i}}{\rho n\omega}\left(\frac{J_0(\beta_n r)}{l\beta_n J_1(\beta_n R)} + 1\right) \mathrm{e}^{\mathrm{i}n\omega t}\right), \tag{31}$$

which corresponds to the case in which the fluid–solid interface is very smooth. Obviously, the velocity profile across the cross-section of the tube tends to be uniform in this case.

Remark 3.3. If $a_0 = -A\epsilon R$, $c_n = 0$ for all $n \geq 1$, and $l = \alpha R/\sqrt{1 - 2\beta}$ (the α and β here refer to the slip parameters defined in Ref. [25]), the solution reduces to a recent result in Ref. [15].

From the above remarks, it is clear that our work generalizes the existing solutions and solves a more general problem.

4. Exact solution of the flow rate and stress field

From the axial velocity solution (29), the flow rate can be determined by

$$\begin{aligned} Q(t) &= \int_0^R 2\pi r u(r,t)\,\mathrm{d}r \\ &= -\frac{a_0\pi R^3}{2\mu}\left(l+\frac{R}{4}\right) - \frac{2\pi}{\rho\omega}\mathrm{Re}\left[\sum_{n=1}^{\infty}\frac{c_n \mathrm{i}\mathrm{e}^{\mathrm{i}n\omega t}}{n}\int_0^R\left(\frac{J_0(\beta_n r)}{J_0(\beta_n R)-l\beta_n J_1(\beta_n R)}-1\right) r\,\mathrm{d}r\right]. \end{aligned} \tag{32}$$

From the identity

$$\frac{\mathrm{d}}{\mathrm{d}x}[xJ_1(x)] = xJ_0(x),$$

we have

$$\frac{\mathrm{d}}{\mathrm{d}r}[rJ_1(\beta_n r)] = \beta_n r J_0(\beta_n r) \tag{33}$$

and hence

$$\int_0^R rJ_0(\beta_n r)\,\mathrm{d}r = \frac{1}{\beta_n}[rJ_1(\beta_n r)]_0^R = \frac{1}{\beta_n}RJ_1(\beta_n R). \tag{34}$$

Thus, by substituting the above formula into (32), we have

$$Q(t) = -\frac{a_0\pi R^3}{2\mu}\left(l+\frac{R}{4}\right) - \frac{2\pi}{\rho\omega}\mathrm{Re}\left\{\sum_{n=1}^{\infty}\frac{c_n \mathrm{i}\mathrm{e}^{\mathrm{i}n\omega t}}{n}\left[\frac{RJ_1(\beta_n R)}{\beta_n[J_0(\beta_n R)-l\beta_n J_1(\beta_n R)]}-\frac{R^2}{2}\right]\right\}. \tag{35}$$

The total amount of fluid passing through the tube during the time period $[0, T]$ can thus be calculated as follows

$$\begin{aligned} Q_T &= \int_0^{\mathrm{T}} Q(t)\,\mathrm{d}t \\ &= -\frac{a_0\pi R^3 T}{2\mu}\left(l+\frac{R}{4}\right) - \frac{2\pi}{\rho\omega^2}\mathrm{Re}\left\{\sum_{n=1}^{\infty}\frac{c_n}{n^2}\left(\mathrm{e}^{\mathrm{i}n\omega T}-1\right)\left[\frac{RJ_1(\beta_n R)}{\beta_n[J_0(\beta_n R)-l\beta_n J_1(\beta_n R)]}-\frac{R^2}{2}\right]\right\}. \end{aligned} \tag{36}$$

Remark 4.1. For the constant component (a_0) of the pressure gradient, the flow rate increases linearly as the slip length l increases. However, for the harmonic components ($c_n\mathrm{e}^{\mathrm{i}n\omega t}$) of the pressure gradient, the relation between the flow rate and the slip length is not immediately clear from the above solution form as it involves a complex parameter and Bessel functions with complex arguments, and so we will further investigate this in Section 5.

In what follows, we will determine the stress field in the fluid. From $\mathbf{v} = \mathbf{e}_r 0 + \mathbf{e}_\theta 0 + \mathbf{e}_z u(r)$ and (5), we obtain

$$\nabla\mathbf{v} = \begin{pmatrix} 0 & 0 & \partial u/\partial r \\ 0 & 0 & 0 \\ \partial u/\partial r & 0 & 0 \end{pmatrix}. \tag{37}$$

From the above formulae and using (4) and (29), we obtain

$$\begin{aligned} &d_{rr} = d_{\theta\theta} = d_{zz} = d_{r\theta} = d_{\theta z} = 0, \\ &d_{rz} = \frac{a_0 r}{2\mu} + \sum_{n=1}^{\infty}\mathrm{Re}\left[\frac{c_n \mathrm{i}}{\rho n\omega}\left(\frac{\beta_n J_1(\beta_n r)}{J_0(\beta_n R)-l\beta_n J_1(\beta_n R)}\right)\mathrm{e}^{\mathrm{i}n\omega t}\right]. \end{aligned} \tag{38}$$

Hence from the constitutive equation (3), we obtain

$$\begin{aligned} &\sigma_{rr} = \sigma_{\theta\theta} = \sigma_{zz} = -p = \bar{q}(t)x + p_0(t), \qquad \sigma_{r\theta} = \sigma_{\theta z} = 0, \\ &\sigma_{rz} = a_0 r + \frac{2\mu}{\rho\omega}\sum_{n=1}^{\infty}\mathrm{Re}\left[\frac{c_n \mathrm{i}}{n}\left(\frac{\beta_n J_1(\beta_n r)}{J_0(\beta_n R)-l\beta_n J_1(\beta_n R)}\right)\mathrm{e}^{\mathrm{i}n\omega t}\right], \end{aligned} \tag{39}$$

where $\bar{q}(t)$ is as given in (11) while $p_0(t)$ is arbitrary and can be chosen to meet certain pressure conditions.

Remark 4.2. For the constant component (a_0) of the pressure gradient, the shear stress in the fluid is independent of the slip length l; while, for the harmonic components ($c_n\mathrm{e}^{\mathrm{i}n\omega t}$) of the pressure gradient, the shear stress is influenced by the slip length.

5. Influence of boundary slip on flow behaviour

With the exact solutions obtained in the previous sections, in this section, we discuss the influences of the slip length on velocity, flow rate and stresses in the fluid. As the solution for a general pressure field is the superposition of the solution due to the constant pressure gradient and the solutions due to the sine and cosine wave pressure gradients, without loss of generality, we consider here two different cases of driving pressure fields. The first case is for a pressure field with a constant pressure gradient, while the second one is for a pressure field with a cosine wave form pressure gradient.

Case 1: $\mathrm{d}p/\mathrm{d}z = a_0$.

For this case, $c_n = 0$ for all $n \geq 1$ and thus, from (29), (35) and (39), we obtain the following normalized velocity, normalized flow rate and normalized shear stress

$$u^* = -\frac{4\mu}{a_0 R^2} u = \left[1 - \left(\frac{r}{R}\right)^2 + \frac{2l}{R}\right] := u^*_{ns} + u^*_{\text{trans}}, \tag{40}$$

$$Q^*(t) = -\frac{2\mu}{a_0 \pi R^3} Q = \left(l + \frac{R}{4}\right), \tag{41}$$

$$\sigma^*_{rz} = \frac{1}{a_0 R}\sigma_{rz} = \frac{r}{R}. \tag{42}$$

Remark 5.1. The normalized velocity consists of two components u^*_{ns} and u^*_{trans}. The first component $u^*_{ns} = 1 - (r/R)^2$ is the solution for the problem under the no-slip condition, namely the no-slip solution, which gives a usual paraboloid velocity profile; while the second component, $u^*_{\text{trans}} = 2l/R$, represents a rigid body translation in the axial direction. Hence, we conclude that the slip solution is simply the superposition of the no-slip solution and a rigid body translation. The magnitude of the rigid body translation velocity is linearly proportional to the slip parameter l. Of course, a rigid body translation will not lead to any change in the material deformation state and stress state. This is why the shear stress in the fluid, in this case, is independent of the slip length and is the same as that predicted by the no-slip condition.

Remark 5.2. The flow rate is linearly propositional to the slip length l. The flow rate - slip length relation (41) can be used to design simple experiments to determine the slip length by measuring the flow rate for a given set of values of μ, R and a_0.

Case 2: $\mathrm{d}p/\mathrm{d}z = a_1 \cos(\omega t)$.

For this case, $a_0 = 0$, $c_1 = a_1 \in R$, $c_n = 0$ for all $n \geq 2$. For convenience in the discussion, we introduce the following dimensionless variables

$$\beta^* = \beta R, \qquad r^* = \frac{r}{R} \in [0, 1], \qquad l^* = \frac{l}{R}, \qquad t^* = \frac{\omega t}{2\pi}, \qquad u^* = -\frac{\rho\omega}{a_1} u. \tag{43}$$

Then, from (29), we obtain

$$u^* = \mathtt{Re}\left[\left(\frac{J_0(\beta^* r^*)}{J_0(\beta^*) - l^*\beta^* J_1(\beta^*)} - 1\right) \mathrm{i}\mathrm{e}^{2\pi t^* \mathrm{i}}\right]. \tag{44}$$

Let

$$A = A(r^*) = \mathtt{Re}\left[\frac{J_0(\beta^* r^*)}{J_0(\beta^*) - l^*\beta^* J_1(\beta^*)}\right], \qquad B = B(r^*) = \mathtt{Im}\left[\frac{J_0(\beta^* r^*)}{J_0(\beta^*) - l^*\beta^* J_1(\beta^*)}\right]. \tag{45}$$

Then

$$\begin{aligned} u^* &= \mathtt{Re}\left[(A + B\mathrm{i} - 1)\left(\cos(2\pi t^*)\mathrm{i} - \sin(2\pi t^*)\right)\right] \\ &= -B\cos(2\pi t^*) + (1 - A)\sin(2\pi t^*). \end{aligned} \tag{46}$$

As the A and B in the above solution form are expressed in terms of the complex parameter β^* and the Bessel functions with complex arguments, it is not immediately clear from this solution form whether the velocity is linearly proportional to l^* or inversely linearly proportional to l^* or is related to l^* nonlinearly. Thus, we first proceed below to derive a more explicit formulae relating u^* and l^* in the real domain. As $\beta^2 = -\frac{\rho\omega}{\mu}\mathrm{i} = \frac{\rho\omega}{\mu}\mathrm{e}^{-\pi\mathrm{i}/2}$, we have

$$\beta = \sqrt{\frac{\rho\omega}{2\mu}}(1 - \mathrm{i}) = \frac{\bar{\beta}}{R}(1 - \mathrm{i}), \qquad \frac{1}{\beta} = \frac{R}{2\bar{\beta}}(1 + \mathrm{i}), \qquad \beta^* = \bar{\beta}(1 - \mathrm{i}), \tag{47}$$

where $\bar{\beta} = R\sqrt{\frac{\rho\omega}{2\mu}}$ is a dimensionless parameter. Further, we let

$$J_0(\beta^*) = \gamma_0 + \lambda_0\mathrm{i}, \qquad J_1(\beta^*) = \gamma_1 + \lambda_1\mathrm{i}, \qquad J_0(\beta^* r^*) = \gamma_{0r} + \lambda_{0r}\mathrm{i}, \tag{48}$$

then

$$\frac{J_0(\beta^* r^*)}{J_0(\beta^*) - l^*\beta^* J_1(\beta^*)} = [\gamma_{0r} + \lambda_{0r}\mathrm{i}]\frac{[\gamma_0 - l^*\bar{\beta}(\gamma_1+\lambda_1)] - [\lambda_0 - l^*\bar{\beta}(\lambda_1-\gamma_1)]\mathrm{i}}{[\gamma_0 - l^*\bar{\beta}(\gamma_1+\lambda_1)]^2 + [\lambda_0 - l^*\bar{\beta}(\lambda_1-\gamma_1)]^2} \tag{49}$$

$$A = \frac{\gamma_{0r}[\gamma_0 - l^*\bar{\beta}(\gamma_1+\lambda_1)] + \lambda_{0r}[\lambda_0 - l^*\bar{\beta}(\lambda_1-\gamma_1)]}{[\gamma_0 - l^*\bar{\beta}(\gamma_1+\lambda_1)]^2 + [\lambda_0 - l^*\bar{\beta}(\lambda_1-\gamma_1)]^2}, \tag{50}$$

$$B = \frac{\lambda_{0r}[\gamma_0 - l^*\bar{\beta}(\gamma_1+\lambda_1)] - \gamma_{0r}[\lambda_0 - l^*\bar{\beta}(\lambda_1-\gamma_1)]}{[\gamma_0 - l^*\bar{\beta}(\gamma_1+\lambda_1)]^2 + [\lambda_0 - l^*\bar{\beta}(\lambda_1-\gamma_1)]^2}. \tag{51}$$

Note that, for $|y| \ll 1$, the following asymptotic formulae, presented in Ref. [35], can be used to approximate Bessel functions

$$J_n(x+y\mathrm{i}) \approx J_n(x) + \frac{\mathrm{i}y}{2}[J_{n-1}(x) - J_{n+1}(x)], \qquad J_n(y) \approx \frac{1}{n!}\left(\frac{y}{2}\right)^n. \tag{52}$$

We thus have, for $\bar{\beta} \ll 1$, the following approximations

$$J_0(\beta^*) = J_0(\bar{\beta} - \bar{\beta}\mathrm{i}) \approx J_0(\bar{\beta}) - \mathrm{i}\frac{\bar{\beta}}{2}[J_{-1}(\bar{\beta}) - J_1(\bar{\beta})] = J_0(\bar{\beta}) + \mathrm{i}\bar{\beta}J_1(\bar{\beta}) \approx 1 + \frac{\bar{\beta}^2}{2}\mathrm{i},$$

$$J_1(\beta^*) = J_1(\bar{\beta} - \bar{\beta}\mathrm{i}) \approx J_1(\bar{\beta}) - \mathrm{i}\frac{\bar{\beta}}{2}[J_0(\bar{\beta}) - J_2(\bar{\beta})] = \frac{\bar{\beta}}{2} - \frac{\bar{\beta}}{2}\left[1 - \frac{\bar{\beta}^2}{8}\right]\mathrm{i},$$

$$J_0(\beta^* r^*) \approx 1 + \frac{\bar{\beta}^2 r^{*2}}{2}\mathrm{i}, \qquad J_1(\beta^* r^*) = \frac{\bar{\beta} r^*}{2} - \frac{\bar{\beta} r^*}{2}\left[1 - \frac{(\bar{\beta} r^*)^2}{8}\right]\mathrm{i}.$$

From the above formulae and (48), we have

$$\gamma_0 = 1, \qquad \lambda_0 = \frac{\bar{\beta}^2}{2}, \qquad \gamma_1 = \frac{\bar{\beta}}{2}, \qquad \lambda_1 = -\frac{\bar{\beta}}{2} + \frac{\bar{\beta}^3}{16}, \qquad \gamma_{0r} = 1, \qquad \lambda_{0r} = \frac{(\bar{\beta} r^*)^2}{2}. \tag{53}$$

Substituting the above into (50) and (51) yields

$$A = \frac{\left[1 - l^*\frac{\bar{\beta}^4}{16}\right] + \frac{(\bar{\beta} r^*)^2}{2}\left[\frac{\bar{\beta}^2}{2} + l^*\bar{\beta}^2\left(1 - \frac{\bar{\beta}^2}{16}\right)\right]}{\left[1 - l^*\frac{\bar{\beta}^4}{16}\right]^2 + \left[\frac{\bar{\beta}^2}{2} + l^*\bar{\beta}^2\left(1 - \frac{\bar{\beta}^2}{16}\right)\right]^2} \approx \frac{1 - \bar{\beta}^4 l^*(1 - 8r^{*2})/16}{1 + \bar{\beta}^4 l^*\left(\frac{7}{8} + l^*\right)} \tag{54}$$

$$B = \frac{-\frac{\bar{\beta}^2}{2}(1 - r^{*2}) - l^*\bar{\beta}^2\left[1 - \frac{\bar{\beta}^2}{16}\left(1 - \frac{(\bar{\beta} r^*)^2}{2}\right)\right]}{\left[1 - l^*\frac{\bar{\beta}^4}{16}\right]^2 + \left[\frac{\bar{\beta}^2}{2} + l^*\bar{\beta}^2\left(1 - \frac{\bar{\beta}^2}{16}\right)\right]^2} \approx -\frac{\bar{\beta}^2(1 - r^{*2} + 2l^*)}{2\left[1 + \bar{\beta}^4 l^*\left(\frac{7}{8} + l^*\right)\right]}. \tag{55}$$

Hence we have

$$u^* \approx \frac{\bar{\beta}^2(1 - r^{*2} + 2l^*)}{2\left[1 + \bar{\beta}^4 l^*\left(\frac{7}{8} + l^*\right)\right]}\cos(2\pi t^*) + \frac{\bar{\beta}^4 l^*(15 - 8r^{*2})/16}{1 + \bar{\beta}^4 l^*\left(\frac{7}{8} + l^*\right)}\sin(2\pi t^*). \tag{56}$$

The above asymptotic expression of the solution clearly shows that the velocity profile at any instant of time is paraboloid on the cross-section of the tube. Fig. 1 shows the velocity profiles at $t^* = n$ for various different values of the slip length, obtained from (56). It is also obvious from the asymptotic expression that the velocity, in this case, is not the simple superposition of the non-slip solution and a rigid body translation velocity. It also shows that the normalized velocity depends only on the dimensionless parameter $\bar{\beta}$ in addition to the slip parameter l^*.

To demonstrate the influence of l^* on the velocity field, we consider here the slip velocity on the wall of the tube $r^* = 1$ at a typical instant of time $t^* = n$ (integer). From (56), the slip velocity on $r^* = 1$ at $t^* = n$ is

$$\frac{u_s^*}{\bar{\beta}^2} = \frac{l^*}{1 + \bar{\beta}^4 l^*\left(\frac{7}{8} + l^*\right)} \tag{57}$$

which clearly indicates that the influence of l^* on the velocity field is nonlinear. From the above formulae, we obtain that,

$$\frac{\partial(u_s^*/\bar{\beta}^2)}{\partial l^*} = 0, \qquad \frac{\partial^2(u_s^*/\bar{\beta}^2)}{\partial l^{*2}} = \frac{-\bar{\beta}^6\left(\frac{7}{3} + 4l^*\right)}{\left[1 + \bar{\beta}^4 l^*\left(\frac{7}{8} + l^*\right)\right]^2} < 0, \quad \text{at } l^* = \frac{1}{\bar{\beta}^2}. \tag{58}$$

Hence, it can be concluded that the slip velocity on the wall achieves its maximum value at $l^* = 1/\bar{\beta}^2$. Fig. 2 shows the influence of the slip length on the slip velocity on the wall. It is clear that the asymptotic formulae provide a very accurate approximation. In the example, we take $\bar{\beta} = 0.02$.

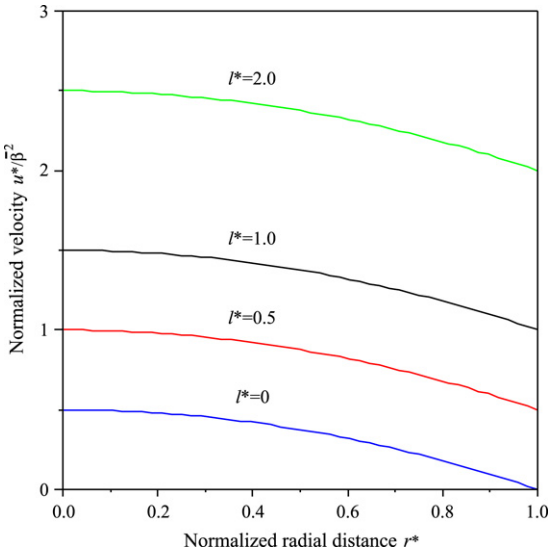

Fig. 1. Velocity profiles for various different values of slip length l^* at a typical instant of time $t^* = n$, obtained from (56) with $\bar{\beta} = 0.02$.

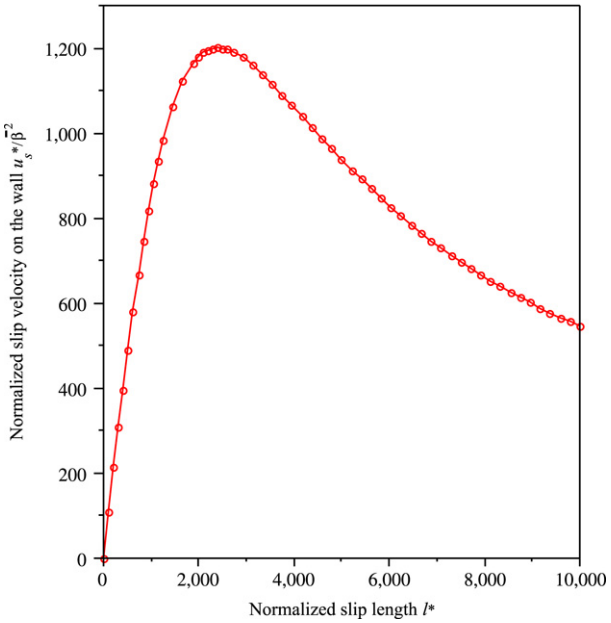

Fig. 2. Influence of slip length l^* on slip velocity on the tube wall. The solid line is obtained from the exact solution (44), while the dots are obtained from the asymptotic solution (57).

Now we consider the flow rate, from (35), we have

$$Q^*(t) = -\frac{\rho\omega\bar{\beta}}{\pi a_1 R^2} Q(t) = \frac{2\bar{\beta}}{R} \mathrm{Re}\left\{ \mathrm{i} e^{2\pi t^* \mathrm{i}} \left[\frac{J_1(\beta^*)}{\beta[J_0(\beta^*) - l^*\beta^* J_1(\beta^*)]} - \frac{R}{2} \right] \right\}. \tag{59}$$

Again, as the solution is expressed in terms of the complex parameter β^* and Bessel functions with complex arguments, it is not immediately clear from this solution form whether the flow rate is linearly proportional to l^*, or inversely linearly proportional to l^* or is related to l^* nonlinearly. Thus, we first proceed below to derive a more explicit formulae relating Q^* and l^* in the real domain.

Let $C = C(1)$, $D = D(1)$ and

$$C(r^*) = \mathrm{Re}\left[\frac{J_1(\beta^* r^*)}{J_0(\beta^*) - l^*\beta^* J_1(\beta^*)} \right], \qquad D(r^*) = \mathrm{Im}\left[\frac{J_1(\beta^* r^*)}{J_0(\beta^*) - l^*\beta^* J_1(\beta^*)} \right]. \tag{60}$$

Then

$$\begin{aligned} Q^*(t^*) &= \mathrm{Re}\left\{\left[(1+\mathrm{i})(C+D\mathrm{i})-\bar{\beta}\right]\left[\mathrm{i}\cos(2\pi t^*)-\sin(2\pi t^*)\right]\right\} \\ &= -(C-D-\bar{\beta})\sin(2\pi t^*)-(C+D)\cos(2\pi t^*). \end{aligned} \tag{61}$$

Noting that

$$\frac{J_1(\beta^*)}{J_0(\beta^*)-l^*\beta^*J_1(\beta^*)} = [\gamma_{1r}+\lambda_{1r}\mathrm{i}]\,\frac{\left[\gamma_0-l^*\bar{\beta}(\gamma_1+\lambda_1)\right]-\left[\lambda_0-l^*\bar{\beta}(\lambda_1-\gamma_1)\right]\mathrm{i}}{\left[\gamma_0-l^*\bar{\beta}(\gamma_1+\lambda_1)\right]^2+\left[\lambda_0-l^*\bar{\beta}(\lambda_1-\gamma_1)\right]^2}, \tag{62}$$

we have, from the definition of C and D, and (60), that

$$\begin{aligned} C+D &= \frac{(\gamma_1+\lambda_1)[\gamma_0-l^*\bar{\beta}(\gamma_1+\lambda_1)]+(\lambda_1-\gamma_1)[\lambda_0-l^*\bar{\beta}(\lambda_1-\gamma_1)]}{[\gamma_0-l^*\bar{\beta}(\gamma_1+\lambda_1)]^2+[\lambda_0-l^*\bar{\beta}(\lambda_1-\gamma_1)]^2} \\ &\approx \frac{-\bar{\beta}^3\left(\frac{7}{16}+l^*\right)}{1+\bar{\beta}^4 l^*\left(\frac{7}{8}+l^*\right)}. \end{aligned} \tag{63}$$

$$\begin{aligned} C-D &= \frac{(\gamma_1-\lambda_1)[\gamma_0-l^*\bar{\beta}(\gamma_1+\lambda_1)]+(\lambda_1+\gamma_1)[\lambda_0-l^*\bar{\beta}(\lambda_1-\gamma_1)]}{[\gamma_0-l^*\bar{\beta}(\gamma_1+\lambda_1)]^2+[\lambda_0-l^*\bar{\beta}(\lambda_1-\gamma_1)]^2} \\ &\approx \frac{\bar{\beta}}{1+\bar{\beta}^4 l^*\left(\frac{7}{8}+l^*\right)}. \end{aligned} \tag{64}$$

Hence, from the above and (46), we obtain the asymptotic expression of the transient flow rate

$$Q^*(t^*) \approx \frac{\bar{\beta}^3\left(\frac{7}{16}+l^*\right)}{1+\bar{\beta}^4 l^*\left(\frac{7}{8}+l^*\right)}\cos(2\pi t^*)+\frac{\bar{\beta}^5 l^*\left(\frac{7}{8}+l^*\right)}{1+\bar{\beta}^4 l^*\left(\frac{7}{8}+l^*\right)}\sin(2\pi t^*). \tag{65}$$

Again, it is interesting to see that $\bar{\beta}$ is the only parameter dominating the normalized flow rate in addition to the slip parameter l^*.

To demonstrate the influence of l^* on the flow rate, we consider a typical instant of time $t^* = n$ (integer) at which

$$\frac{Q^*(n)}{\bar{\beta}^3} \approx \frac{\frac{7}{16}+l^*}{1+\bar{\beta}^4 l^*\left(\frac{7}{8}+l^*\right)}, \tag{66}$$

which clearly indicates that the influence of l^* on the flow rate is nonlinear. It is easy to show that at $l^* = 1/\bar{\beta}^2 - 7/16$, the first-order derivative of $Q^*(n)$ vanishes and the second-order derivative is negative. Hence $Q^*(n)$ achieves its maximum value at $l^* = 1/\bar{\beta}^2 - 7/16$. Fig. 3 shows the variation of the flow rate with l^* at $t^* = n$.

In the following, we consider the stress field in the fluid. From (39), we obtain the normalized stress as follows

$$\begin{aligned} \sigma_{rz}^* &= -\frac{\rho\omega R}{2\mu a_1\bar{\beta}}\sigma_{rz} = -\frac{R}{\bar{\beta}}\mathrm{Re}\left[\frac{\beta J_1(\beta^* r^*)}{J_0(\beta^*)-l^*\beta^*J_1(\beta^*)}\mathrm{i}e^{2\pi t^*\mathrm{i}}\right] \\ &= -\mathrm{Re}\left\{(1-\mathrm{i})\left[C(r^*)+D(r^*)\mathrm{i}\right]\left[\mathrm{i}\cos(2\pi t^*)-\sin(2\pi t^*)\right]\right\} \\ &= \left[C(r^*)+D(r^*)\right]\sin(2\pi t^*)+\left[D(r^*)-C(r^*)\right]\cos(2\pi t^*). \end{aligned} \tag{67}$$

To see the influence of l^* on the flow rate, we consider a typical instant of time $t^* = n + 1/4$ (n is an integer). Following the same procedure as that used for the flow rate, we obtain

$$\bar{\sigma}_{rz}(r^*) = -\frac{\sigma_{rz}^*(r^*)}{\bar{\beta}^3} = -\frac{C(r^*)+D(r^*)}{\bar{\beta}^3} \approx \frac{r^*(8-r^{*2}+16l^*)/16}{1+\bar{\beta}^4 l^*\left(\frac{7}{8}+l^*\right)}. \tag{68}$$

Hence the maximum shear stress, which occurs on the wall surface $r^* = 1$, is

$$\bar{\sigma}_{rz}(1) \approx \frac{(7/16+l^*)}{1+\bar{\beta}^4 l^*\left(\frac{7}{8}+l^*\right)}.$$

Obviously, as discussed before, $\bar{\sigma}_{rz}(1)$ achieves its maximum value at $l^* = 1/\bar{\beta}^2 - 7/16$. The influence of l^* on the normalized maximum shear stress $\bar{\sigma}_{rz}(1)$ on the wall is as that shown in Fig. 3.

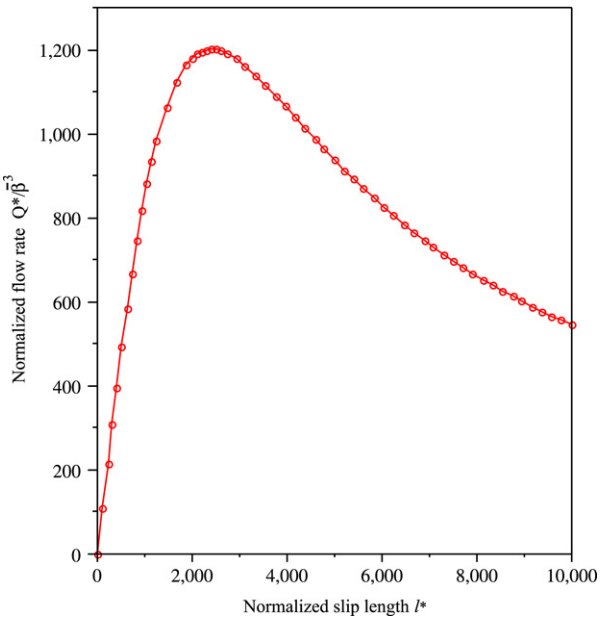

Fig. 3. Influence of slip length l^* on flow rate. The solid line is obtained from the exact solution (59), while the dots are obtained from the asymptotic solution (66).

6. Conclusions

In this paper, we derive an exact solution for the transient flow of an incompressible Newtonian fluid in microtubes with a Navier slip condition on the boundary. Based on the solution derived, we analyse the influence of the slip parameter on velocity and flow rate as well as stress field in the fluid. The findings from the work and their significance are summarized as follows.

(i) The study shows that the influences of boundary slip on the flow behaviour are qualitatively different for different types of pressure fields driving the flow. For pressure fields with a constant pressure gradient, the boundary slip does not alter the interior material deformation and stress field, as it only causes the addition of an axial rigid body translation velocity onto the no-slip solution. However, for the pressure field with a wave form pressure gradient, the influence of boundary slip on the flow is much more complex. The boundary slip causes the change of interior material deformation and consequently the velocity profile and stress field.

(ii) For the case of constant pressure gradient, a simple explicit formula (41) has been derived relating the flow rate with the slip length, which can be used as a basis for designing simple experiments to determine the slip length.

(iii) For the flow driven by a cosine wave form pressure gradient, by deriving an asymptotic expression for the solution, we found that the parameter $\bar{\beta}$ dominates the normalized velocity and the normalized flow rate as well as the normalized stress. We also found that the slip velocity attains its maximum value when $l^* = 1/\bar{\beta}^2$, while the flow rate at $t^* = n + 1/4$ achieves its maximum value at $l^* = 1/\bar{\beta}^2 - 7/16$.

(iv) The exact solutions of the velocity and flow rate as well as stress field provide explicit analytical formulae describing the flow behaviour, which provides a basis for designing microtubes and driving pressure field to optimally control the transient velocity profile and flow rate as well as stress field in the fluid. In addition, the exact solutions also provide a tool for validating numerical methods developed for solving no-slip problems for which no exact solution is available, as it is always useful to check the numerical method against the exact solution for a solved problem of similar type before applying the method to study unsolved problems.

Acknowledgements

The first author is grateful to the financial support of the Australian Research Council through a discovery project grant. The second author gratefully acknowledges the support of Mahidol University and the Thailand Research Fund (TRF). The authors are also grateful to the referees whose comments have led to a number of significant improvements.

References

[1] B. Bourlon, J. Wong, C. Miko, Nanoscale probe for fluidic and ionic transport, Nature Nanotechnology 2 (2) (2007) 104.

[2] B.Y. Cao, M. Chen, Z.Y. Goo, Velocity slip of liquid flow in nanochannels, Acta Physica Sinica 55 (10) (2006) 5305.
[3] B.Y. Cao, M. Chen, Z. Guo, Liquid flow in surface-nanostructured channels studied by molecular dynamics simulation - art. no. 066311, Physical Review E 7406 (6) (2006) 6311.
[4] M. Carpinlioglu, M. Gundogdu, A critical review on pulsatile pipe flow studies directing towards future research topics, Flow Measurement and Instrumentation 12 (2001) 163.
[5] G. Chauveteau, Rodlike polymer solution flow through fine pores: influence of pore size on rheological behavior, Journal of Rhelogy 26 (2) (1982) 111.
[6] S.R. Deshmukh, D.G. Vlachos, CFD simulations of coupled, countercurrent combustor/reformer microdevices for hydrogen production, Industrial & Engineering Chemistry Research 44 (14) (2005) 4982.
[7] M. Gad-el-Hak, The fluid mechanics of microdevices—The Freeman scholar lecture, Journal of Fluids Engineering-Transactions of the ASME 121 (1) (1999) 5.
[8] H. Herwig, O. Hausner, Critical view on new results in micro-fluid mechanics: An example, International Journal of Heat and Mass Transfer 46 (5) (2003) 935.
[9] C.M. Ho, Y.C. Tai, Micro-electro-mechanical systems (MEMS) and fluid flows, Annual Review of Fluid Mechanics 30 (1998) 579.
[10] H. Huang, T.S. Lee, C. Shu, Lattice Boltzmann method simulation gas slip flow in long microtubes, International Journal of Numerical Methods for Heat & Fluid Flow 17 (5–6) (2007) 587.
[11] Peter Huang, Kenneth S. Breuer, Direct measurement of slip length in electrolyte solutions, Physics of Fluids 19 (2007) 028104.
[12] T.C. Kuo, D.M. Cannon, M.A. Shannon, P.W. Bohn, J.V. Sweedler, Hybrid three-dimensional nanofluidic/microfluidic devices using molecular gates, Sensors and Actuators, A 102 (2003) 223.
[13] L. Eric, M.S. Todd, Brownian motion near a partial-slip boundary: A local probe of the no-slip condition, Physics of Fluids 17 (2005) 103102.
[14] H.B. Lee, I.W. Yeo, K.K. Lee, Water flow and slip on NAPL-wetted surfaces of a parallel-walled fracture - art. no. L19401, Geophysical Research Letters 34 (19) (2007) 19401.
[15] M.T. Matthews, J.M. Hill, Newtonian flow with nonlinear Navier boundary condition, Acta Mechanica 191 (3–4) (2007) 195.
[16] J.J. Nakane, M. Akeson, A. Marziali, Nanopores sensors for nucleic acid analysis, Journal of Physics Condensed Matter 15 (2005) R1365.
[17] J.P. Pascal, Instability of power-law fluid flow down a porous incline, Journal of Non-Newtonian Fluid Mechanics 133 (2–3) (2006) 109.
[18] R. Pit, H. Hervet, L. Leger, Direct experimental evidence of slip in hexadecane: Solid interfaces, Physical Review Letters 85 (2000) 980.
[19] S. Ray, B. Unsal, F. Durst, O. Ertunc, O.A. Bayoumi, Mass flow rate controlled fully developed laminar pulsating pipe flows, Journal of Fluids Engineering 127 (2005) 405.
[20] K.C. Sahu, P. Valluri, P.D.M. Spelt, O.K. Matar, Linear instability of pressure-driven channel flow of a Newtonian and a Herschel–Bulkley fluid, Physics of Fluids 19 (2007) 122101.
[21] F. Saidi, Non-Newtonian flow in a thin film with boundary conditions of Coulomb's type, Zamm-Zeitschrift Fur Angewandte Mathematik Und Mechanik 86 (9) (2006) 702.
[22] J.C. Slattery, Advanced Transport Phenomena, Cambridge University Press, 1999.
[23] Y.C. Su, L.W. Lin, A water-powered micro drug delivery system, Journal of Microelectromechanical Systems 13 (1) (2004) 75.
[24] L. Szalmas, Slip-flow boundary condition for straight walls in the lattice Boltzmann model - art. no. 066710, physical Review E 7306 (6) (2006) 6710.
[25] P.A. Thompson, S.M. Troian, A general boundary condition for liquid flow at solid surfaces, Nature 389 (1997) 360.
[26] R. Tuinier, T. Taniguchi, Polymer depletion-induced slip near an interface, Journal of Physics Condensed Matter 17 (2005) L9.
[27] L. De Vargas, O. Manero, On the slip phenomenon of polymeric solutions through capillaries, Polymer Engineering and Science 29 (18) (1989) 1232.
[28] B. Wiwatanapataphee, Y.H. Wu, J. Archapitak, P.F. Siew, B. Unyong, A numerical study of the turbulent flow of molten steel in a domain with a phase-change boundary, Journal of Computational and Applied Mathematics 166 (2004) 307.
[29] B. Wiwatanapataphee, D. Poltem, Y.H. Wu, Y. Lenbury, Simulation of pulsatile flow of blood in stenosed coronary artery bypass with graft, Mathematical Biosciences and Engineering 3 (2) (2006) 371.
[30] Y.H. Wu, B. Wiwatanapataphee, Modelling of turbulent flow and multi-phase heat transfer under electromagnetic force, Discrete and Continuous Dynamical Systems-Series B 8 (3) (2007) 695.
[31] J.L. Xu, Y.X. Li, Boundary conditions at the solid-liquid surface over the multiscale channel size from nanometer to micron, International Journal of Heat and Mass Transfer 50 (13–14) (2007) 2571–2581.
[32] S.P. Yang, K.Q. Zhu, Analytical solutions for squeeze flow of Bingham fluid with Navier slip condition, Journal of Non-Newtonian Fluid Mechanics 138 (2–3) (2006) 173.
[33] Y. Christophe, B. Catherine, Cottin-Bizonne Ćcile, Joseph Pierre, Bocquet Lyd́ric, Achieving large slip with superhydrophobic surfaces: Scaling laws for generic geometries, Physics of Fluids 19 (2007) 123601.
[34] Y. Donghyun, M. Parviz, Effects of hydrophobic surfaces on the drag and lift of a circular cylinder, Physics of Fluids 19 (2007) 081701.
[35] H.A. Yousif, R. Melka, Bessel function of the first kind with complex argument, Computer Physics Communications 106 (1997) 199.
[36] Y.X. Zhu, S. Granick, Rate-dependent slip of Newtonian liquid at smooth surfaces - art. no. 096105, Physical Review Letters 8709 (9) (2001) 6105.